Techno-Economic Analysis of Redox Flow Batteries with Thermal Coupling under Dynamic Tariffs

Lixin Li, Felix Schofer, Lakshimi Narayanan Palaniswamy,
Anna Sina Starosta, Bernhard Schwarz, Nina Munzke, Marc Hiller
Institute of Electrical Engineering, Karlsruhe Institute of Technology (KIT), Karlsruhe, Germany,
*lixin.li@kit.edu

***Abstract*—The increasing share of renewable energy in Germany has intensified electricity price volatility, underscoring the economic potential of energy storage solutions as energy buffers. This study proposes a techno-economic framework to evaluate vanadium redox flow batteries (VRFBs) under dynamic electricity tariffs and photovoltaic (PV) surplus scenarios. The framework integrates an electro-thermal VRFB model with mixed-integer linear programming (MILP) to identify optimal system configurations and operation strategies. Using real load data from a university building, the economic performance of VRFB-only systems and VRFB systems coupled with thermal coupling modules (TCMs) is assessed. Results show that a 50 kWh VRFB with a 75 kW TCM yields a net present value (NPV) of €55,000, while the VRFB-only system achieves an NPV of –€11,000. These findings demonstrate that thermal integration significantly enhances the economic viability of VRFB-based storage solutions.**

***Index Terms*—redox flow battery, electro-thermal model, mixed-integer linear programming, techno-economic analysis, dynamic tariff.**

I. Introduction

The growing share of renewable energy sources in electricity generation has led to increasing price volatility in electricity markets. In Germany, renewables accounted for 62.7% of total electricity generation in 2024 [1], resulting in 457 hours of negative wholesale electricity prices due to supply-demand mismatches [2]. These dynamics underscore the need for energy storage systems (ESSs) that enable time-of-use optimization by shifting electricity consumption from high-price to low-price periods.

Industrial and commercial consumers, which constitute a major portion of total energy demand, typically require two distinct forms of energy: thermal energy, primarily for space and water heating, and electrical energy, for powering lighting, appliances, and equipment [3]. While lithium-ion batteries (LIBs) are widely adopted for electrical load management, they offer limited support for integrated thermal applications. In contrast, vanadium redox flow batteries (VRFBs), though less commercially widespread, exhibit inherent thermal characteristics. A VRFB is a type of rechargeable electrochemical ESS that uses two liquid electrolyte solutions containing dissolved redox-active species to store energy [4]. On the one hand, a VRFB requires a large electrolyte volume because of low energy density. On the other hand, energy losses during operation are transferred into the electrolyte. These two characteristics make VRFBs promising candidates for dual-purpose storage when combined with thermal coupling modules (TCMs).

Despite this potential, the coordinated use of VRFBs for both electrical and thermal energy management remains underexplored. To address this gap, this study conducts a techno-economic analysis comparing VRFB-only systems with electro-thermal VRFB systems integrated with TCMs. The main contributions of this paper are as follows:

- A simplified electro-thermal VRFB model, calibrated using real-world data, is developed.
- The economic potential of electro-thermal VRFB systems for large-scale consumers is investigated, focusing on electricity and heating cost savings and improved photovoltaic (PV) self-consumption.
- The sizing and operational strategies of VRFB-only and VRFB+TCM systems are optimized and compared to determine the most cost-effective configuration.

II. Problem Description

Fig. 1 presents a simplified schematic of energy flows within a university building equipped with a VRFB system. In this diagram, blue and orange arrows denote electrical and thermal energy flows, respectively. The building's electricity demand is met by the power grid, a set of PV panels, and the VRFB system. Thermal energy is primarily provided by district heating, with the VRFB system acting as a supplementary thermal energy storage solution.

When integrated with a TCM, the VRFB system adopts a dual-loop thermal architecture. In the primary loop, water circulates through immersed heat exchangers within the electrolyte tanks to extract waste heat from the electrolyte. To utilize surplus PV energy, electric heating elements are incorporated into the primary loop to generate thermal energy via Joule heating, which is then either retained within the electrolyte or transferred to the secondary loop. The secondary loop transfers the captured thermal energy to a hot water storage tank serving the building's heating demands. This architecture ensures physical isolation between the two loops, thereby preventing cross-contamination risks.

This study conducts a techno-economic analysis of VRFB systems in the aforementioned application. As illustrated in Fig. 2, an optimization framework is established to enhance the system's techno-economic performance. By iteratively executing the optimization and analysis procedures through varying

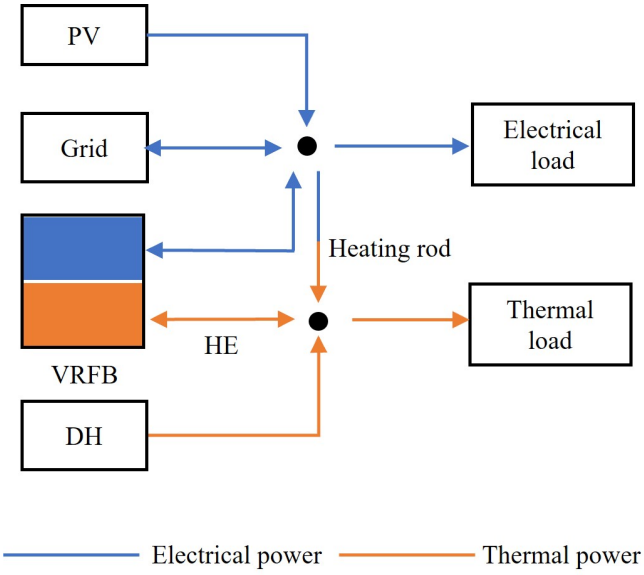

Fig. 1. Energy flow diagram for a university building. DH is short for district heating, and HE is short for heat exchanger. This diagram combines multiple heat exchangers in the TCM into one for simplicity.

combinations of key system parameters (VRFB capacity and TCM rated power), the net present value (NPV) is systematically evaluated. The most cost-effective system configuration is ultimately identified by comparing NPV outcomes across all parameter combinations.

NPV is a fundamental financial metric used to assess the profitability of an investment by discounting future cash flows to their present value. It accounts for both initial capital costs and projected future revenues and expenses, adjusting them based on the time value of money. The NPV is computed as follows:

$$NPV = \sum_{y=1}^{Y} \frac{C_y}{(1+r)^y} - C_0, \tag{1a}$$

$$C_y = R_y - O_y, \tag{1b}$$

where y, Y, C_y, r, C_0, R_y, O_y define the year index, total lifetime, net cash flow, discount rate, initial investment, revenue, and operating cost.

III. System Modeling

A system model is developed to formulate the optimization problem for coordinated energy scheduling. First, a general electrical model of the VRFB system is presented, along with the corresponding power balance constraints. Subsequently, a thermal storage model is established, and the associated thermal power balance equations are derived to enable electro-thermal coupling strategies.

A. Electrical energy system modeling

The ESS within the power nodes framework [5] over a discrete time horizon $\mathcal{T} = \{1, \cdots, N\}$ can be mathematically

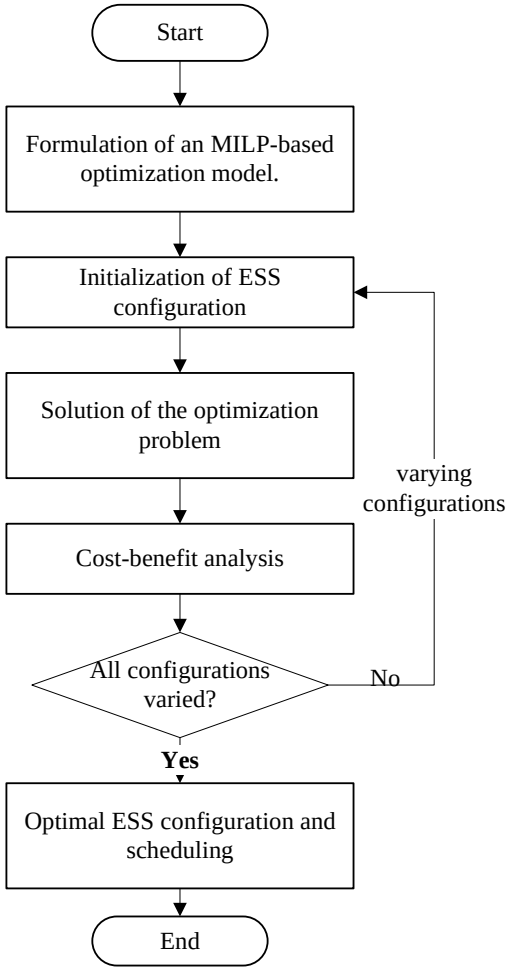

Fig. 2. Framework for techno-economic analysis.

formulated as follows:

$$x_b^{\text{ele}}(t) = x_b^{\text{ele}}(t-1) - \frac{\Delta t}{E_b^{\text{ele}}} P_b^{\text{ele}}(t), \ \forall t \in \mathcal{T}, \tag{2a}$$

$$P_b^{\text{ele}}(t) = \eta^{-1} P_{\text{b,dhg}}^{\text{ele}}(t) - \eta P_{\text{b,chg}}^{\text{ele}}(t), \ \forall t \in \mathcal{T}, \tag{2b}$$

The parameters Δt, E_b^{ele}, and η represent the time step, the energy capacity, and the charge/discharge efficiency of the ESS, respectively. The ESS power is denoted as $P_b^{\text{ele}}(t)$, comprising the discharge power $P_{\text{b,dhg}}^{\text{ele}}(t)$ and charge power $P_{\text{b,chg}}^{\text{ele}}(t)$ at the bus interface. The variable $x_b^{\text{ele}}(t)$ denotes the battery's energy state at time t. The stored energy in the ESS is constrained within predefined lower and upper bounds, given by:

$$\underline{x}_b^{\text{ele}} \le x_b^{\text{ele}}(t) \le \overline{x}_b^{\text{ele}}, \ \forall t \in \mathcal{T}, \tag{3}$$

where $\bar{\cdot}$ and $\underline{\cdot}$ define the respective upper and lower limits. Similarly, the constraints on charging and discharging operations are formulated as:

$$0 \le P_{\text{b,chg}}^{\text{ele}}(t) \le \delta_{\text{b,chg}}(t) \overline{P}_{\text{b}}, \ \forall t \in \mathcal{T}, \tag{4a}$$

$$0 \le P_{\text{b,dhg}}^{\text{ele}}(t) \le \delta_{\text{b,dhg}}(t) \overline{P}_{\text{b}}, \ \forall t \in \mathcal{T}, \tag{4b}$$

$$0 \le \delta_{\text{b,chg}}(t) + \delta_{\text{b,dhg}}(t) \le 1, \ \forall t \in \mathcal{T}, \tag{4c}$$

where binary variables $\delta_{\text{b,chg}}(t)$ and $\delta_{\text{b,dhg}}(t)$ can be incorporated to ensure that the ESS does not engage in simultaneous charging and discharging [6].

B. Electrical power balance

The electrical power balance of the whole system in Fig. 1 is formulated as follows:

$$\begin{aligned} P^{\text{ele}}_{\text{ht}}(t) = P^{\text{ele}}_{\text{g}}(t) + P^{\text{ele}}_{\text{b,dhg}}(t) - P^{\text{ele}}_{\text{b,chg}}(t) \\ + P^{\text{ele}}_{\text{pv}}(t) - P^{\text{ele}}_{\text{d}}(t),\ \forall t \in \mathcal{T}, \end{aligned} \tag{5a}$$

$$P^{\text{ele}}_{\text{g}}(t) = P^{\text{ele}}_{\text{g,takeout}}(t) - P^{\text{ele}}_{\text{g,feedin}}(t),\ \forall t \in \mathcal{T}, \tag{5b}$$

where $P^{\text{ele}}_{\text{ht}}(t)$, $P^{\text{ele}}_{\text{g}}(t)$, $P^{\text{ele}}_{\text{d}}(t)$, $P^{\text{ele}}_{\text{pv}}(t)$ represent electrical power of the heating rod, the grid-side power, the demand, and the PV generation at time t, respectively. The grid power $P^{\text{ele}}_{\text{g}}(t)$ is further decomposed into the grid extraction power $P^{\text{ele}}_{\text{g,takeout}}(t)$ and the grid feed-in power $P^{\text{ele}}_{\text{g,feedin}}(t)$ to account for the price difference between buying and selling electricity. Similar to the ESS power, the limits on the grid out-take and feed-in are formulated as follows:

$$0 \le P^{\text{ele}}_{\text{g,takeout}}(t) \le \delta_{\text{g,takeout}}(t)\overline{P}_{\text{g}},\ \forall t \in \mathcal{T}, \tag{6a}$$

$$0 \le P^{\text{ele}}_{\text{g,feedin}}(t) \le \delta_{\text{g,feedin}}(t)\overline{P}_{\text{g}},\ \forall t \in \mathcal{T}, \tag{6b}$$

$$0 \le \delta_{\text{g,takeout}}(t) + \delta_{\text{g,feedin}}(t) \le 1,\ \forall t \in \mathcal{T}. \tag{6c}$$

C. Thermal energy system modeling

Similar to electrical state of energy (SoE) $x^{\text{ele}}_b(t)$, we introduce a thermal SoE $x^{\text{tm}}_b(t)$, defined by the normalized electrolyte temperature:

$$x^{\text{tm}}_b(t) = \frac{T(t) - T_{\min}}{T_{\max} - T_{\min}}, \tag{7}$$

where $T(t)$ is the electrolyte temperature, $T_{\min}$ and $T_{\max}$ represent the system's allowed lower and upper temperature limits, respectively. Therefore, the thermal dynamics of the VRFB can be modelled as:

$$\begin{aligned} x^{\text{tm}}_b(t) = x^{\text{tm}}_b(t-1) \\ + \frac{\Delta t}{m_b c_b \Delta T_b}(P^{\text{tm}}_b(t) - P^{\text{tm}}_{\text{exg}}(t)),\ \forall t \in \mathcal{T}, \end{aligned} \tag{8a}$$

$$\begin{aligned} P^{\text{tm}}_b(t) = (\eta_{\text{pcs}} - \eta)P^{\text{ele}}_{\text{b,chg}}(t) + (\eta^{-1} - \eta^{-1}_{\text{pcs}})P^{\text{ele}}_{\text{b,dhg}}(t) \\ + c_{\text{ec}}(P^{\text{ele}}_{\text{b,chg}}(t) - P^{\text{ele}}_{\text{b,dhg}}(t)) \\ + c_{\text{aux}}(P^{\text{ele}}_{\text{b,chg}}(t) + P^{\text{ele}}_{\text{b,dhg}}(t)) \\ - c_{\text{abt}}E^{\text{ele}}_{\text{b}},\ \forall t \in \mathcal{T}, \end{aligned} \tag{8b}$$

where m_b, c_b, and ΔT_b represent the electrolyte mass and its specific heat capacity, and the permissible temperature range, respectively. The product $m_b c_b \Delta T_b$ corresponds to the system's maximum usable thermal energy capacity. The thermal SoE, as defined in (8a), is determined by the internal thermal variation within the electrolyte, $P^{\text{tm}}_b(t)$, and the thermal energy exchange with the coupling heat exchanger, $P^{\text{tm}}_{\text{exg}}(t)$. As shown in (8b), $P^{\text{tm}}_b(t)$ consists of charge/discharge losses on the battery side (terms 1 and 2), where η_{pcs} represents the converter efficiency, entropic heat resulting from internal electrochemical reactions (term 3), auxiliary device dissipation involved in the charging/discharging process (term 4), and ambient heat loss (term 5).

D. Thermal power balance

The thermal power balance of the whole system in Fig. 1 is formulated as follows:

$$P^{\text{tm}}_{\text{d}}(t) = P^{\text{tm}}_{\text{exg}}(t) + P^{\text{tm}}_{\text{dh}}(t) + P^{\text{ele}}_{\text{ht}}(t),\ \forall t \in \mathcal{T}, \tag{9a}$$

$$-x^{\text{tm}}_b(t)\overline{P}^{\text{tm}}_{\text{exg}} \le P^{\text{tm}}_{\text{exg}}(t) \le x^{\text{tm}}_b(t)\overline{P}^{\text{tm}}_{\text{exg}},\ \forall t \in \mathcal{T}, \tag{9b}$$

$$0 \le P^{\text{tm}}_{\text{dh}}(t) \le \overline{P}^{\text{tm}}_{\text{d}},\ \forall t \in \mathcal{T}, \tag{9c}$$

where $P^{\text{tm}}_{\text{d}}(t)$ represents the total thermal demand, which is satisfied through thermal output from the VRFB via the heat exchanger $P^{\text{tm}}_{\text{exg}}(t)$, thermal input from the district heating network $P^{\text{tm}}_{\text{dh}}(t)$, and heat generated by the electric heating rod $P^{\text{ele}}_{\text{ht}}(t)$. This model combines multiple heat exchangers in the TCM into one for simplicity. The thermal output $P^{\text{tm}}_{\text{exg}}(t)$ is dynamically regulated by both its instantaneous thermal SoE and the maximum heat transfer capacity of the heat exchanger.

IV. Optimal Operation for VRFB

The VRFB system in Fig. 1 serves two primary functions. First, it stores surplus PV generation in the form of electrochemical and thermal energy. Second, it performs load shifting through time-of-use optimization. These functionalities contribute to increased PV self-consumption and a reduced average electricity purchase price, thereby lowering overall electricity costs.

In the following, two operating modes of the VRFB system are introduced: (1) BESS only, and (2) BESS with TCM.

A. BESS only

When the VRFB is used solely as an electrical ESS, only its electrical layer operation needs to be considered. The optimal operation problem is formulated as follows:

$$\begin{aligned} \min_{\mathbf{P}^{\text{ele}}_{\text{b}}, \mathbf{P}^{\text{ele}}_{\text{g}}} \ & \sum_{t \in \mathcal{T}} \Delta t (c^{\text{ele}}_{\text{buy}}(t) P^{\text{ele}}_{\text{g,takeout}}(t) - c^{\text{ele}}_{\text{sell}} P^{\text{ele}}_{\text{g,feedin}}(t)), \\ \text{s.t.} \ & \text{ESS electrical model: (2), (3), (4),} \\ & \text{Electrical power balance: (5), (6),} \end{aligned} \tag{10}$$

where $c^{\text{ele}}_{\text{buy}}(t)$, $c^{\text{ele}}_{\text{sell}}$ represent the dynamic electricity buying price and the PV feed-in price. Variables in bold $\mathbf{P}$ stand for the stacked power across the period $\mathcal{T}$. In this mode, the power of the heating rod $P^{\text{ele}}_{\text{ht}}(t)$ is set to zero.

B. BESS with TCM

The integration of a VRFB with a TCM enables bidirectional thermal energy utilization: waste heat recovery from electrolyte circulation and active conversion of surplus PV

TABLE I
SUMMARY OPTIMIZATION SETUP

Objects	Parameters	Values	Units
Profiles	Electrical load	212	MWh
	Thermal load	381	MWh
	PV generation	225	MWh
	Average electricity price[1]	0.3	€/kWh
	District heating price[2]	0.17	€/kWh
	Electricity feed-in price[3]	0.06	€/kWh
VRFB[4]	Size	100 / 25	kWh/kW
	Total installed cost	736	€/kWh
	Fixed O&M	6.8	€/kW-a
	Life year	15	a
	RTE η^2	0.7	-
	Converter efficiency η_{pcs}	0.95	-
	Electrical SoE limit	[0.1, 0.9]	-
VRFB (thermal)[5]	Entropic heat coefficient c_{ec}	0.27	-
	Pump loss coefficient c_{aux}	$\frac{1}{14}$	-
	Ambient loss coefficient c_{abt}	0.01	h^{-1}
	Temperature limit	$[10, 40]$	°C
	Thermal SoE limit	$[0, 1]$	-
TCM	Heat exchanger	50	kW
	System price[6]	7500	€
Optimization	Simulation time span	1	a
	Sampling time Δt	1	h
	Initial electrical SoE	0.1	-
	Initial thermal SoE	0.5	-

[1] Dynamic electricity price contracts can be obtained from providers such as *GP JOULE* [8]. The real-time electricity price equals the EPEX market price plus a base price.
[2] The district heating price is based on statistics from the German Verbraucherzentrale.
[3] The feed-in tariff for PV is determined by the German Bundesnetzagentur [9].
[4] The technical and economic parameters of VRFB are sourced from PNNL [10].
[5] The heat-related parameters are obtained from the measurements of the "BiFlow" project [11] and then scaled.
[6] The offer is based on the BiFlow project construction estimate of €15,000 per 100 kW, scaled accordingly.

generation into thermal energy. In this context, the optimization simultaneously considers both the electrical and the thermal layer, as formulated below:

$$\begin{aligned}\min_{\substack{\mathbf{P}^{\text{ele}}_{\text{b}},\mathbf{P}^{\text{ele}}_{\text{g}},\mathbf{P}^{\text{ele}}_{\text{ht}},\\ \mathbf{P}^{\text{tm}}_{\text{exg}},\mathbf{P}^{\text{tm}}_{\text{dh}}}} & \sum_{t\in\mathcal{T}} \Delta t(c^{\text{ele}}_{\text{buy}}(t)P^{\text{ele}}_{\text{g,takeout}}(t) - c^{\text{ele}}_{\text{sell}}P^{\text{ele}}_{\text{g,feedin}}(t) \\ & + c^{\text{ht}}_{\text{buy}}P^{\text{ht}}_{\text{dh}}(t)), \\ \text{s.t.}\ & \text{ESS electrical model: (2), (3), (4),} \\ & \text{Electrical power balance: (5), (6),} \\ & \text{ESS thermal model: (7), (8),} \\ & \text{Thermal power balance: (9).}\end{aligned} \tag{11}$$

where $c^{\text{ht}}_{\text{buy}}$ represents the district heating price.

The above two optimization problems are solved using off-the-shelf optimizers such as *Gurobi* [7].

V. RESULTS AND ANALYSIS

This section applies the proposed design framework to a use case. The electrical and thermal load profiles of a university building [12] are considered, along with real-world PV generation data obtained from the project "Solar Park" [13] at the Karlsruhe Institute of Technology (KIT). The three annual profiles are illustrated in Fig. 3, and their key parameters are summarized in Table I.

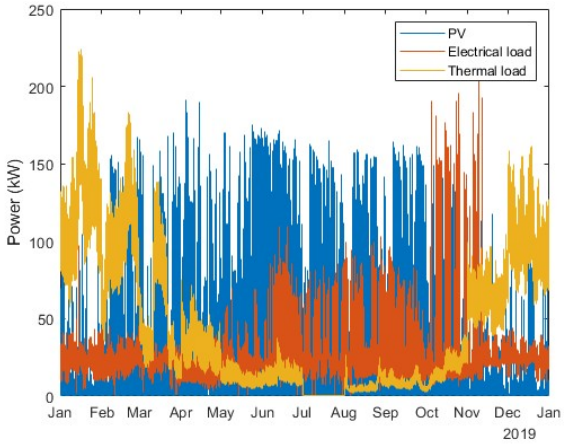

Fig. 3. The annual profiles of PV generation, electrical load, and thermal load.

The analysis begins with a comparison between two system configurations: a 100 kWh VRFB system and a 100 kWh VRFB system integrated with a 50 kW TCM, as summarized in Table I. This comparison evaluates the coordinated benefits of electro-thermal coupling. Subsequently, a parametric optimization is performed over a multi-dimensional design space defined by varying VRFB capacities (50–200 kWh) and TCM power ratings (25–100 kW). The optimal configuration is identified by maximizing the NPV.

A. Operation analysis

Since visualizing one year long data is challenging, the following analysis focuses on the optimization results for one representative day.

1) Operation of VRFB-only: Fig. 4 illustrates the optimized operation of the VRFB-only system. In Fig. 4(a), bars above the x-axis represent the power injected into the system, while bars below the x-axis indicate the power consumed by the system. The bars are symmetric to the x-axis, reflecting instantaneous power balance. The gray line represents the dynamic electricity price throughout the day.

From $00:00$ to $05:00$, PV generation is negligible, and the entire load demand is met by the grid due to low electricity prices during this period. Between $05:00$ and $18:00$, PV generation sufficiently covers the electrical load. The surplus PV power is initially fed into the grid, and then it is simultaneously used for grid feed-in and VRFB charging. After $18:00$, PV generation stops and electricity prices increase sharply. The VRFB discharges to supply the electrical load, reducing grid dependency during high-price hours.

Under this scenario, the VRFB is used solely as an electrical ESS. Consequently, the building's thermal demand is fully supplied by the district heating network.

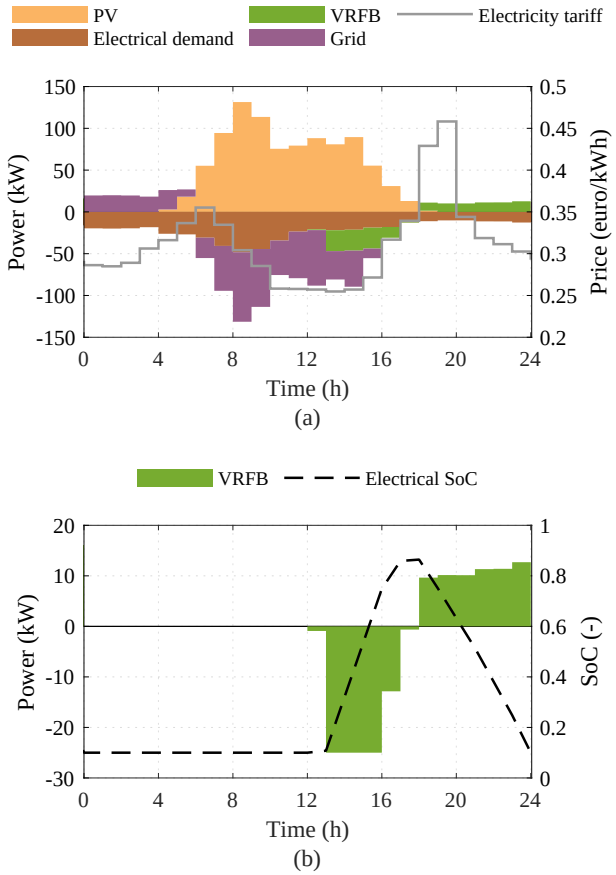

Fig. 4. Optimized operation for VRFB on the observation day. (a) Total power distribution. (b) VRFB power and electrical SoE.

2) Operation of VRFB with TCM: The optimized operation of the VRFB system with the TCM is analyzed and illustrated in Fig. 5. The left column presents the operation results of the electrical layer, while the right column displays those of the thermal layer.

The electrical operation, shown in Fig. 5(a) and Fig. 5(b), resembles that of the previous scenario. Between 00 : 00 and 05 : 00, the electrical load is primarily supplied by the grid. Between 05 : 00 and 18 : 00, PV generation is first used to supply the electrical load and drive the heating rod for thermal energy production. Any remaining surplus PV energy is subsequently used to charge the VRFB and feed into the grid. After 18 : 00, the VRFB discharges during the high-price period to meet the electrical load and reduce grid dependency.

The thermal operation, presented in Fig. 5(c) and Fig. 5(d), shows that during morning and evening hours, the VRFB continuously provides thermal power. The thermal demand gap during these periods is covered by district heating. When PV generation is sufficient, the heating rod is activated to satisfy thermal demand while simultaneously heating the electrolyte tanks. In this way, thermal demand is met by PV generation through the electro-thermal VRFB system, reducing reliance on district heating.

B. Economic analysis of different configurations

NPVs are calculated for VRFB-only and VRFB-TCM under different system sizes. The results demonstrate strict economic infeasibility of VRFB-only configurations, with negative NPV persisting across all capacity ranges. Table II summarizes NPV performance for VRFB-TCM systems, in which the rows represent different battery sizes, and the columns represent different TCM sizes. The table indicates that, when a 50 kWh VRFB system is coupled with a 75 kW TCM, it achieves the highest NPV of €55,000.

Table III details the economic performance of this optimal configuration. Compared to the VRFB-only, the VRFB-TCM system demonstrates an annual revenue of approximately 8 k€ through multi-vector energy dispatch. With a 15-year lifecycle analysis at a 2% discount rate, this configuration achieves an NPV of €55,000, representing much higher than that of the VRFB-only system with NPV of -€11,000.

TABLE II
NPV RESULTS FOR DIFFERENT VRFB AND COUPLING MODULE SIZES. ALL VALUES ARE IN THOUSANDS OF EUROS (K€).

VRFB \ TCM	25kW	50kW	75kWh	100kW
50kWh	43	54	**55**	54
100kWh	30	43	45	44
150kWh	5	15	17	16
200kWh	−29	−21	−20	−23

TABLE III
COMPARISON OF NPV ACROSS THREE SCENARIOS

Metrics	Benchmark	VRFB[3]	VRFB-TCM[4]
Grid usage (MWh/a)	118	109	109
District heating (MWh/a)	381	380	329
PV feed-in (MWh/a)	131	118	69
PV SCR[1](%)	42	48	70
Initial investiment (k€)	0	37	48
Maintenance (k€/a)	0	0.1	0.1
Electricity charges (k€/a)	38	35	35
Heating charges (k€/a)	65	65	56
Feed-in revenue (k€/a)	8	7	4
Annual revenue[2](k€/a)	-	1.9	8
NPV (k€)	-	−11	55

[1] SCR is short for self-consumption rate.
[2] Annual revenue is defined as the difference between the annual operating costs of the benchmark system and those of the VRFB-TCM system.
[3] The optimized VRFB-only system of 50 kWh capacity.
[4] The optimized 50 kWh VRFB system with 75 kW TCM.

VI. SUMMARY AND FUTURE WORKS

This paper presents a techno-economic analysis framework for VRFB deployment in a university building, designed to optimize system configuration under dynamic electricity pricing and PV surplus conditions. The proposed framework integrates a simplified electro-thermal storage model and utilizes MILP to optimize system operation, aiming to minimize electricity and heating costs. By evaluating NPVs of different system configurations, the framework determines the optimal VRFB-TCM system and its corresponding operation strategy.

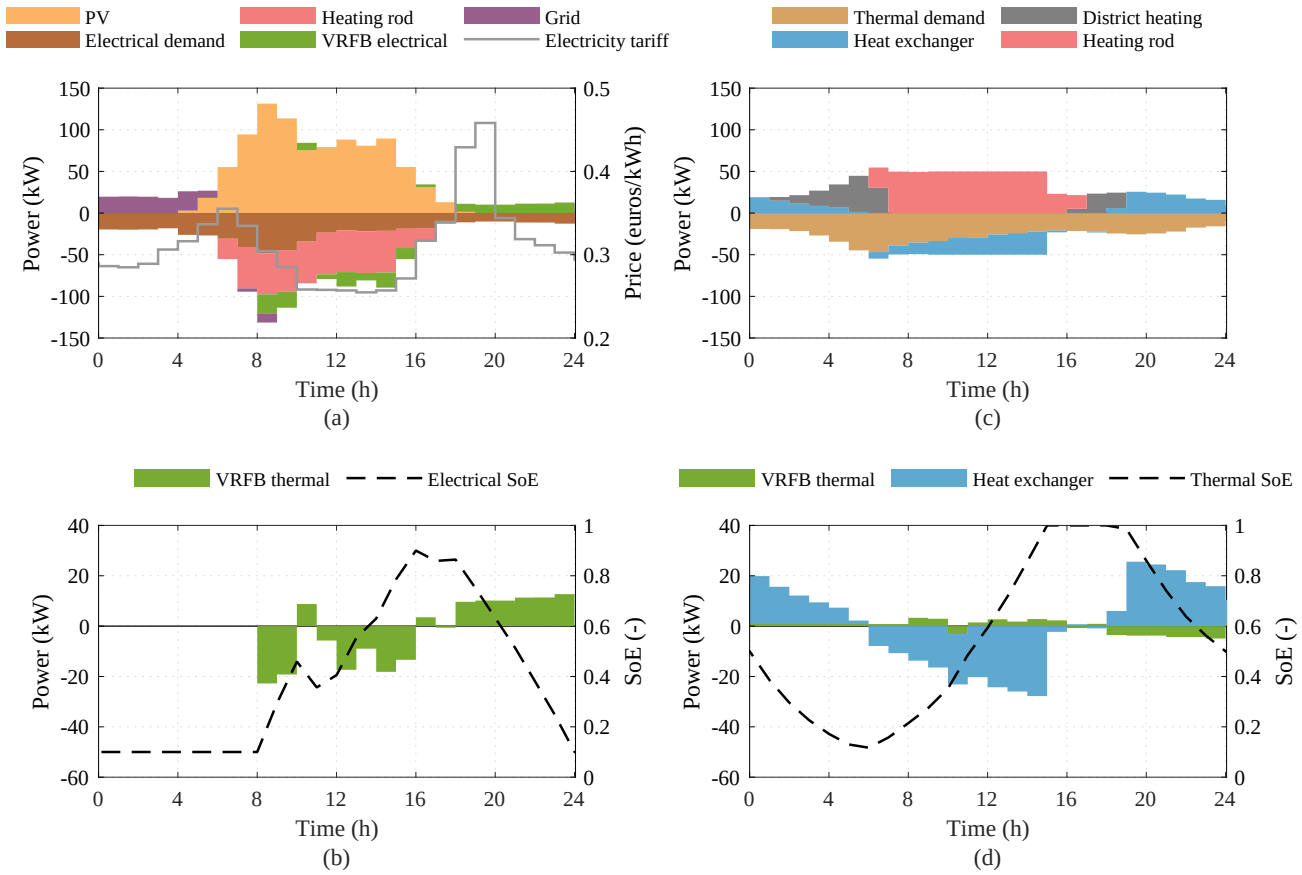

Fig. 5. Optimized operation for VRFB with TCM on the observation day. (a) Electrical power distribution. (b) VRFB electrical power and electrical SoE. (c) Thermal power distribution. (b) VRFB thermal power and thermal SoE.

Future research will focus on developing a more detailed nonlinear VRFB model and exploring heuristic optimization methods.

References

[1] "Public Electricity Generation 2024: Renewable Energies cover more than 60 Percent of German Electricity Consumption for the First Time - Fraunhofer ISE," Jan. 2025. [Online]. Available: https://www.ise.fraunhofer.de/en/press-media/press-releases/2025.html

[2] T. Hamlyn, "Germany records 457 hours of negative electricity prices in 2024," PV Magazine, Jan. 2025, [Online]. Available: https://www.pv-magazine.com/2025/01/06/germany-records-457-hours-of-negative-electricity-prices-in-2024/.

[3] "Energy consumption and use by households." [Online]. Available: https://ec.europa.eu/eurostat/web/products-eurostat-news/-/ddn-20200626-1

[4] N. Poli, C. Bonaldo, M. Moretto, and M. Guarnieri, "Techno-economic assessment of future vanadium flow batteries based on real device/market parameters," *Applied Energy*, vol. 362, p. 122954, May 2024. [Online]. Available: https://linkinghub.elsevier.com/retrieve/pii/S0306261924003374

[5] K. Heussen, S. Koch, A. Ulbig, and G. Andersson, "Unified system-level modeling of intermittent renewable energy sources and energy storage for power system operation," *IEEE Systems Journal*, vol. 6, no. 1, pp. 140–151, 2011.

[6] L. Li, A. S. Starosta, B. Schwarz, N. Munzke, H.-M. Strehle, M. Richter, and M. Hiller, "Optimal design of energy storage system for peak-shaving in industrial production," in *NEIS 2023; Conference on Sustainable Energy Supply and Energy Storage Systems*. VDE, 2023, pp. 79–85.

[7] Gurobi Optimization, LLC, "Gurobi Optimizer Reference Manual," 2024. [Online]. Available: https://www.gurobi.com

[8] "GP JOULE flex - Der dynamische Stromtarif von GP JOULE." [Online]. Available: https://content.energymarket.solutions/gp-joule/was-ist-ein-dynamischer-tarif/

[9] "Bundesnetzagentur - EEG-Förderung und -Fördersätze." [Online]. Available: https://www.bundesnetzagentur.de/DE/Fachthemen/ElektrizitaetundGas/ErneuerbareEnergien/EEG_Foerderung/start.html

[10] "Energy Storage Cost and Performance Database," publisher: Pacific Northwest National Laboratory. [Online]. Available: https://www.pnnl.gov/projects/esgc-cost-performance

[11] L. N. Palaniswamy, N. Munzke, C. Kupper, and M. Hiller, "Optimized energy management of a solar and wind equipped student residence with innovative hybrid energy storage and power to heat solutions," in *International Renewable Energy Storage Conference (IRES 2022)*. Atlantis Press, 2023, pp. 363–382.

[12] D. Let, "University campus buildings electrical and thermal demand and generation." Nov. 2022. [Online]. Available: https://zenodo.org/records/7371390

[13] T. Kappler, A. S. Starosta, B. Schwarz, N. Munzke, and M. Hiller, "Inclusion of shading and soiling with physical and data-driven algorithms for solar power forecasting," in *PV-Symposium Proceedings*, vol. 1, 2024.